PROCEEDINGS OF SCIENCE

Propagating Air Shower Radio Signals to In-ice Antennas

Uzair Abdul Latif,[a,*] **Tim Huege,**[a,b] **Krijn de Vries,**[a] **Simon de Kockere,**[a] **Dieder Van den Broeck**[a] **and Stijn Buitink**[a]

[a] *Vrije Universiteit Brussel (VUB),*
Pleinlaan 2, Brussels, Belgium
[b] *Karlsruhe Institute of Technology (KIT),*
PO Box 3640, 76021 Karlsruhe, Germany
E-mail: uzair.abdul.latif@vub.be, tim.huege@kit.edu, krijn.de.vries@vub.be, simon.de.kockere@vub.be, dieder.van.den.broeck@vub.be, stijn.buitink@vub.be

Cosmic ray showers can serve as important calibration sources for in-ice radio detectors aiming to detect the cosmic neutrino flux at the highest energies. However, if not well understood, radio emissions from cosmic ray showers pose an essential background signal in the neutrino search. Thus, we have adapted the CoREAS air shower radio emission simulation code to simulate air shower radio signals for in-ice antennas. We present a novel upgrade CoREAS such that it takes into account curved ray paths caused by the exponential refractive index profiles of air and ice. This enables propagating signals from air to antennas located inside the ice sheets.

9th International Workshop on Acoustic and Radio EeV Neutrino Detection Activities - ARENA2022
7-10 June 2022
Santiago de Compostela, Spain

*Speaker

PoS(ARENA2022)016

1. Introduction

In-ice Askaryan radio experiments like ARA, RNO-G, and ARIANNA have deployed radio antennas inside the Greenlandic and Antarctic ice sheets [1–3]. These in-ice radio experiments are looking to measure the flux of cosmogenic and astrophysical neutrinos at even higher energies than IceCube ($> 10^{17}$ eV). The in-ice radio detectors are designed to record and measure coherent radio Cherenkov emission, known as Askaryan emission, from the particle cascade induced by the neutrino-ice nuclei collision.

Radio emissions from particle cascades, dubbed extensive air showers, induced by ultra-high energy cosmic rays interacting in the atmosphere serve as essential backgrounds for Askaryan radio detectors. Arriving with a relatively high flux, cosmic ray particle cascades produce radio signals with many similar features compared to neutrino signals. As such, cosmic rays provide the ideal calibration signal if their signal is understood and can be separated from the neutrino signal. The effort to fully characterize cosmic-ray signals observed by in-ice radio detectors is underway and will be the goal of this work. However, it should be noted that this work will be limited to in-air radio emissions. In contrast, the in-ice emission when the cosmic-ray shower propagates into the ice sheet will be discussed in another work [4, 5].

In this work, cosmic-ray air shower radio emission will be simulated with CoREAS (CORSIKA-based Radio Emission from Air Showers) [6]. CoREAS is a sub-module of the CORSIKA (COsmic Ray SImulations for KAscade) air shower simulation [7]. CoREAS uses the endpoint formalism to calculate the electric field emission from each shower particle (as simulated by CORSIKA) as the shower propagates and makes no assumptions regarding the emission mechanism. However, the CoREAS code has only been designed to work in air using straight-line ray propagation. In reality, air and ice have density-dependent exponential refractive index profiles that cause radiowave rays to curve as they propagate toward an observer. The ray-bending effect is much less pronounced for air than ice since, in polar ice, the refractive index refractive has an exponential profile which has a large gradient in the first 100 – 200 m. Polar ice refractive index changes from 1.35 at the surface to 1.78 within 100 – 200 m, and the sharp change in the refractive index causes the rays to bend significantly near the ice surface.

2. Refractive Index Profiles of Air and Ice

The ice refractive index profile in the polar regions can be parameterized in the form of:

$$n(z) = A + B\exp(-Cz) \tag{1}$$

Here the values of the A, B and C parameters uniquely define the refractive index profile of a given medium. A is the asymptotic refractive index value. In the case of polar ice, z will be the depth below the ice surface, and for air, z becomes the altitude (h) of a point above the ice surface.

In the case of ice, the parameters will be defined as $A = 1.78$, $B = -0.43$ and $C = -0.0132\,\mathrm{m}^{-1}$. These parameter values are for the South Pole ice profile and are also used by the ARA and RICE experiments [8].

In air, obtaining the refractive index model becomes slightly more complex. CORSIKA works with a 5-layer atmosphere profile when it simulates particle cascades; therefore, our air refractive

index profile will have the same structure with each layer having the exponential form as given by Eq. 1 [7].

CORSIKA comes with a GDAS tool (Global Data Assimilation System) that constructs an atmosphere profile by considering the corresponding density and humidity profile for a specific location and time [9]. At the same time, CoREAS receives a consistent, tabular refractivity profile from GDAS that also considers humidity effects when calculating the refractive index profile [9].

The GDAS tabulated refractive index model generally follows an exponential trend but is not smooth. In order to do raytracing we need to 'construct' a 5-layer refractive index profile with each layer having a smooth exponential profile (equivalent to Eq. 1). The five exponential layers are constructed by using the value of the C parameter (provided by GDAS tool) and the value of the refractive index at sea level and assuming that the asymptotic value of each refractive index profile is 1. The A, B and C parameter values obtained for each atmosphere layer for a location close to the South Pole are given in Table 1.

Layer	Altitude Range (m)	A	B	C (m^{-1})
1	0 to 3217.48	1	0.000328911	0.000123309
2	3217.48 to 8363.54	1	0.000348817	0.000141571
3	8363.54 to 23141.80	1	0.000361006	0.000145679
4	23141.80 to 100000	1	0.000368118	0.000146522
5	$>$ 100000	1	0.000368117	0.000146522

Table 1: A, B and C parameters obtained for the refractive index profile of air for a location close to the South Pole.

3. Raytracing from Air to Ice

In this work, we trace the path of radiowaves as they propagate through air and ice. To do so, we use analytic expressions for raytracing that depend on smooth exponential refractive index profiles of any given medium [10, 11].

Four ingredients are needed in order to define a geometry for raytracing: 1. $\mathrm{THD}_{\mathrm{Total}}$, the Total Horizontal Distance between the emission point and the observer 2. h, the altitude of the emission point in air 3. z, the depth of the antenna 4. The ice layer altitude. In order to obtain raytracing parameters like the ray propagation time, path length, etc., from the analytic raytracing expressions, one is required to provide the initial launch angle of the ray. At the correct launch angle, the ray will hit the target point in ice. Therefore, raytracing involves a minimization procedure. In order to acquire the 'correct' launch angle, the following expression will be minimized:

$$f(\theta, h, z) = \mathrm{THD}_{\mathrm{Air}}(\theta, h) + \mathrm{THD}_{\mathrm{Ice}}(\theta, z) - \mathrm{THD}_{\mathrm{Total}} \tag{2}$$

In Eq. 2 we are performing the minimization over $\mathrm{THD}_{\mathrm{Total}}$ of the ray in air and ice using the fact that at the correct launch angle the $\mathrm{THD}_{\mathrm{Air}}$, the Total Horizontal Distance traveled by the ray in air, and $\mathrm{THD}_{\mathrm{Ice}}$, the Total Horizontal Distance traveled by the ray in ice, should add up to be $\mathrm{THD}_{\mathrm{Total}}$. It should be noted that Eq. 2 is a function of θ (the launch angle), h and z, which are set by the initial geometry chosen by a user. Minimization is then performed and θ is varied until $f(\theta, h, z) < \epsilon$, with a tolerance level ϵ. The 'correct' launch angle can then be used to obtain the ray parameters for the given geometry.

3.1 Interpolation

A typical call to the analytic raytracing functions involving air and ice takes around 0.05 – 0.1 ms. This is relatively fast but not fast enough for simulating a whole cosmic ray shower. A typical cosmic-ray shower will consist of $O(10^9)$ particles at EeV energies. In this case, propagating rays from each shower particle at each step to each antenna could take weeks or months, depending on the shower energy and the number of in-ice antennas. Therefore, it is not feasible to use the analytic raytracing functions directly, and we have to move towards interpolation.

Interpolation of ray parameters from pre-made tables makes the raytracing process considerably faster. The interpolation tables are made in the following way:

1. For each in-ice antenna depth, a 2-D grid is created with variables h and $\mathrm{THD}_{\mathrm{Total}}$.
    - h is varied from 3000 m to 100000 m covering airshower altitudes for a 3 km high ice layer.
    - $\mathrm{THD}_{\mathrm{Total}}$ is varied by varying the ray launch angle (θ) from 89.9° (almost horizontal) to 0° (vertically down). Small variations in θ can cause almost exponential changes in $\mathrm{THD}_{\mathrm{Total}}$.
2. Each grid position describes a unique geometry for raytracing. For each geometry, the following parameters are obtained and stored:
    - The initial launch angle of the ray
    - The total optical and geometric path length of the ray in air and in ice.
    - $\mathrm{THD}_{\mathrm{Air}}$ and $\mathrm{THD}_{\mathrm{Ice}}$
    - The angle of incidence of the ray on the ice surface and the corresponding Fresnel coefficients.

The tables are then used to supply CoREAS with the ray parameters for any given geometry that CoREAS encounters by using linear interpolation between the grid values. Each interpolation call for a given parameter takes around 250 ns, making the raytracing process significantly faster and as such air shower radio emission calculations in gradient media feasible. An important thing to note regarding raytracing is that it is performed in the context of a 'flat Earth' and is thus applicable to air showers with zenith angles of up to $\sim 65°$. Beyond a zenith angle of 65°, it becomes important to take Earth's curvature into account.

3.2 Interpolation Results

Fig. 1 contains several plots which help quantify the results of interpolation for the $\mathrm{THD}_{\mathrm{Air}}$ ray parameter. In Fig. 1 we plotted the emission altitude h on the x-axis and Γ on the y-axis. As defined in Fig. 1d, Γ is the straight-line angle between an in-air transmitter and the in-ice receiver, $\Gamma = 180$ means vertically down, and $\Gamma = 90$ means pointing horizontally outwards. It should be noted the $\mathrm{THD}_{\mathrm{Air}}$ grid patterns are practically identical between Fig. 1a (raytraced results) and Fig. 1b (interpolated results). Fig. 1c shows the error for the interpolated results is around $O(10^{-5}\% - 10^{-6}\%)$. It can also be noted that in the bottom left corner of Fig. 1a and Fig. 1b, there is a small region where there are no raytracing solutions. This is because of the presence of a shadow zone in air due to the ray bending in exponential refractive index profiles.

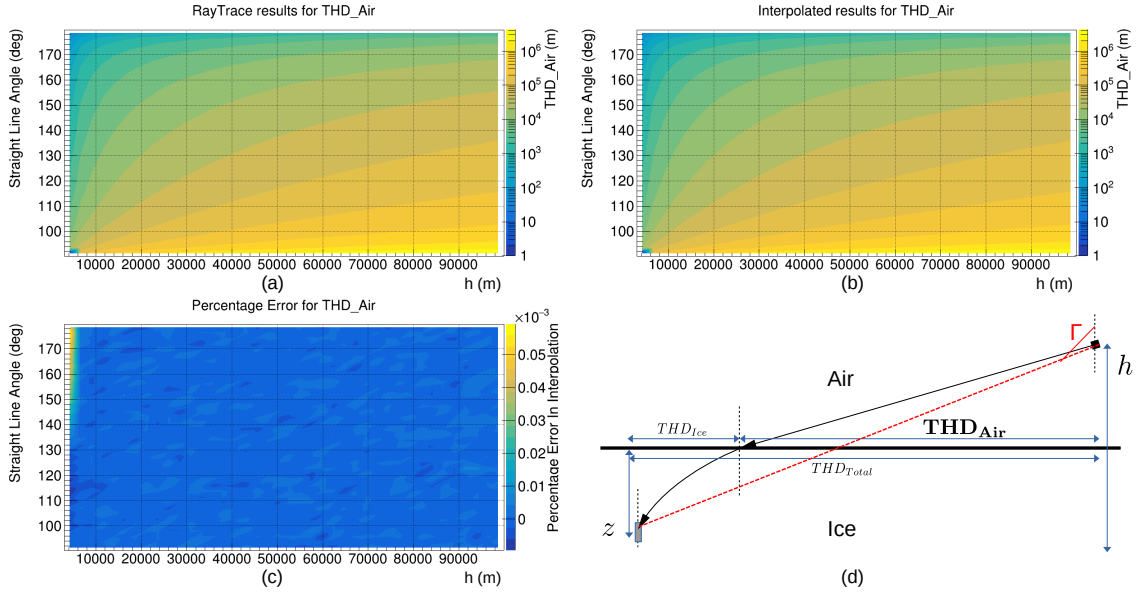

Figure 1: This figure contains several plots to quantify the performance of the interpolation, focusing solely on the interpolation of the THD_{Air} parameter. On the x-axis, we plot the emission altitude h, and on the y-axis, we plot the straight line angle Γ, defined in Fig. 1d. Fig. 1a shows the results for raytracing, Fig. 1b shows the results for interpolation, Fig. 1c shows the percentage error in interpolation along the whole grid and Fig. 1d shows the schematic for the whole setup.

4. Raytracing in CoREAS

Incorporating raytracing parameters in CoREAS is relatively straightforward. CoREAS works with the following expression to calculate the electric field emissions from individual particles [12]:

$$\vec{E}(\vec{x},t) = \frac{q}{c}\left[\frac{\hat{r}\times[(\hat{r}-n\vec{\beta})\times\dot{\vec{\beta}}]}{(1-n\vec{\beta}.\hat{r})^3\,R}\right]_{\text{ret}} \tag{3}$$

In order to perform raytracing, Eq. 3 gets modified in the following way:

1. the angle of the $\vec{\beta}.\hat{r}$ dot product is replaced with the launch angle obtained from raytracing.
2. R gets replaced with the value of the geometrical path length of the ray in air and ice.
3. the value of n is taken to be the refractive index value at the emission point.

Modifications 1 and 3 have been discussed in detail in another work [13]. It has been shown that these modifications align with physics and allow for the 'correct' integration of raytracing in CoREAS.

It should also be noted that Fresnel coefficients have not been included in the electric field calculations as of yet, although they are being calculated by the raytracer. This is foreseen in the near future.

4.1 Results

All cosmic-ray showers that will be discussed in this section were simulated with CoREAS using the following settings:

1. *THINNING* was set to be *ON* in order to have reasonable simulation times. The thinning threshold was set at 1×10^{-6} with the maximum weight being 100.
2. The energy of the primary particle was set to be 1×10^{17} eV.
3. The zenith and azimuth angles were set to be at 0° (i.e. the direction of the shower was vertically downwards).
4. Whenever the showers were simulated using in-ice antennas, the altitude of the ice sheet was fixed to be 3000 m.

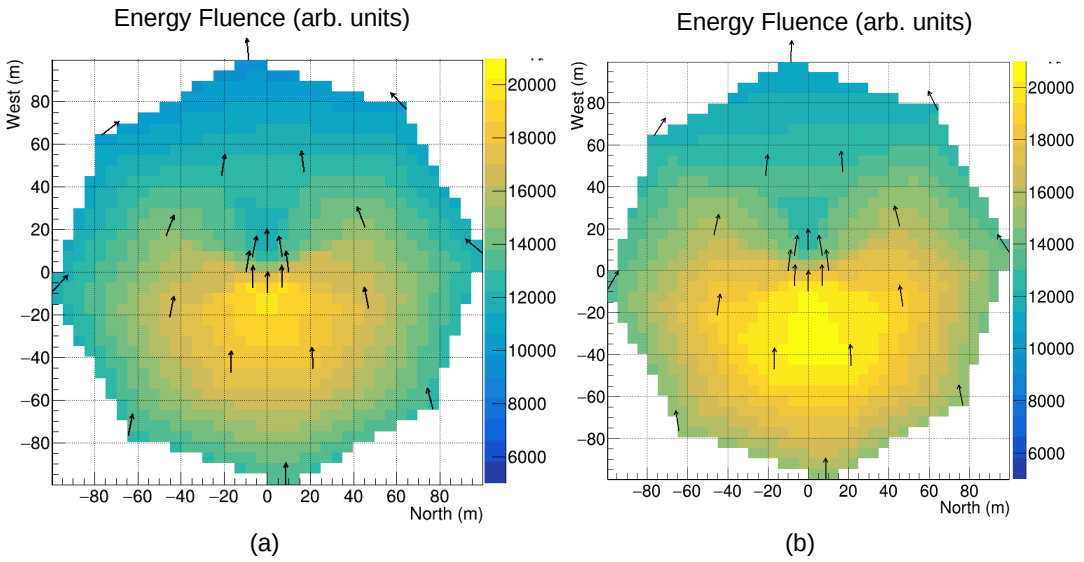

Figure 2: In-ice (Fig. 2a) and in-air (Fig. 2b) shower radio footprints. Antennas were placed in a plane in a circular configuration, and their positions are indicated by the position of the arrows. The altitude of antennas is 2900 m and is the same for both cases, but for Fig. 2a, the presence of an ice sheet at 3000 m puts the antennas 100 m in depth below the surface. The direction of the arrows indicates the direction of electric field polarisation as observed in the horizontal plane. The colour scale on the z-axis shows the energy fluence observed at each point.

Cosmic-ray shower radio footprints are shown in Figs. 2a (in-ice) and 2b (in-air). The simulated electric field pulses at each antenna location, indicated by the arrow positions, were used to calculate the total energy fluence. The entire footprint was then generated using 2-D interpolation between the antenna positions. First, we notice the anisotropy in received power across the footprint caused by the interference between Askaryan and geomagnetic emission mechanisms [14]. It is also observed that the total power received in-ice is significantly less than in-air. The reduction of electric field strength at the in-ice antennas is caused partly by ray bending due to rays being refracted in ice, partly by reflection loss at the air-ice boundary and also because, currently, our calculations lack a focusing factor correction. The focusing factor correction has been discussed in detail in another publication [15]. Part of the loss in electric field magnitude can also be attributed to rays which come at an angle beyond the critical angle and hence, get totally internally reflected in air and do

not penetrate the ice sheet. Here it should be noted that the so-called focusing effect is not included in these simulations.

The direction of the arrows at the antenna positions in Figs. 2a and 2b indicate the direction of polarization of the electric field in the horizontal plane. In Fig. 2b, most of the arrows point West as that is the direction of geomagnetic emission ($-\vec{v} \times \vec{B}$). Some arrows located at antenna positions on the outer edge of the footprint point towards the side as the Askaryan emission starts to dominate and the power received is considerably less at those points. In Fig. 2a the rays got refracted into the ice, and most of the power in the footprint gets focused towards the centre. Therefore for antenna positions further away from the centre, Askaryan emission is relatively enhanced, and the arrows start to point towards the centre of the footprint. The electric field waveforms from the simulated

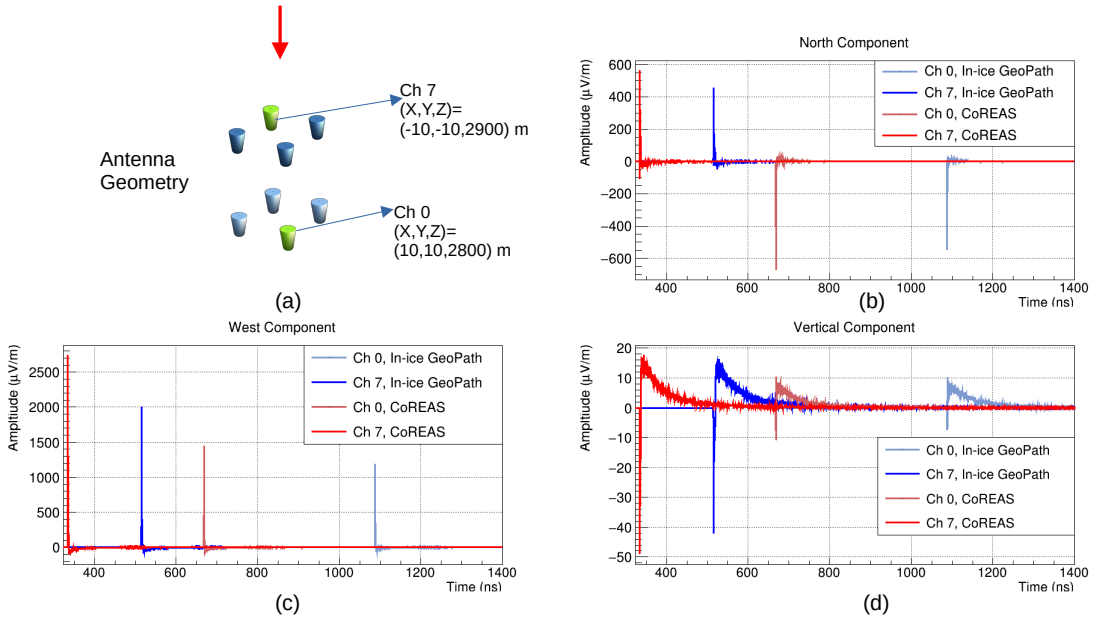

Figure 3: The observed electric field pulses at two antenna locations. Antennas Ch. 7 and Ch. 0 were selected, and their positions are indicated in Fig. 3a. Fig. 3b, Fig. 3c and Fig. 3d show the waveforms for the North, West and Vertical electric field components respectively. For each component, we compare electric field pulses observed in case the antennas are positioned in ice (dark blue for Ch. 7 and light blue Ch. 0) and in the case where no ice is present the antennas are located in air (red for Ch. 7 and magenta for Ch. 0).

cosmic ray showers are shown in Figs. 3b, 3c and 3d for the North, West and Vertical components of the electric field. The two antenna positions used for obtaining the electric field waveforms are indicated in the schematic in Fig. 3a. As expected, the electric field pulses arrive with a delay in ice compared to air. As discussed earlier, the overall observed amplitude is scaled down. It should also be noted that the pulse shape remains consistent between the in-ice and in-air simulations.

5. Conclusion

We have fully integrated analytic raytracing in CoREAS that now accounts for exponential refractive index profiles of air and ice. The interpolation code introduced to do raytracing is fast enough to allow the CoREAS simulations to finish in a reasonable amount of time. The following steps will be to integrate the calculation of the Fresnel coefficients and simulate in-air and in-ice

emissions, the latter originating from cosmic-ray air showers penetrating a high-altitude ice sheet, in one simulation.

References

[1] ARA Collaboration collaboration, *Constraints on the diffuse flux of ultrahigh energy neutrinos from four years of askaryan radio array data in two stations*, *Phys. Rev. D* **102** (2020) 043021.

[2] J. Aguilar, P. Allison, J. Beatty, H. Bernhoff, D. Besson, N. Bingefors et al., *Design and sensitivity of the radio neutrino observatory in greenland (RNO-g)*, *Journal of Instrumentation* **16** (2021) P03025.

[3] A. Anker, S. Barwick, H. Bernhoff, D. Besson, N. Bingefors, D. García-Fernández et al., *Probing the angular and polarization reconstruction of the ARIANNA detector at the south pole*, *Journal of Instrumentation* **15** (2020) P09039.

[4] S. De Kockere, K. de Vries, U. Latif and N. van Eijndhoven, *Simulation of the propagation of cosmic ray air shower cores in ice*, in *9th International Workshop on Acoustic and Radio EeV Neutrino Detection Activities — PoS ARENA2022 (2022) 015*, vol. 424.

[5] S. De Kockere, K.D. de Vries, N. van Eijndhoven and U.A. Latif, *Simulation of in-ice cosmic ray air shower induced particle cascades*, *Phys. Rev. D* **106** (2022) 043023.

[6] T. Huege, M. Ludwig and C.W. James, *Simulating radio emission from air showers with CoREAS*, *AIP Conf. Proc.* **1535** (2013) 128 [1301.2132].

[7] D. Heck, J. Knapp, J.N. Capdevielle, G. Schatz and T. Thouw, *CORSIKA: A Monte Carlo code to simulate extensive air showers*, *FZKA* **6019** (1998) .

[8] J. Kelley, M.-Y. Lu, D. Seckel, Y. Pan, D.Z. Besson and F.T.A. Collaboration, *Observation of two deep, distant (1.4, 4)km impulsive RF transmitters by the Askaryan Radio Array (ARA).*, *PoS* **ICRC2017** (2018) 1030.

[9] P. Mitra, A. Bonardi, A. Corstanje, S. Buitink, G. Krampah, H. Falcke et al., *Reconstructing air shower parameters with lofar using event specific gdas atmosphere*, *Astroparticle Physics* **123** (2020) 102470.

[10] U.A. Latif, *Towards measurement of UHECR with the ARA experiment*, Ph.D. thesis, University of Kansas, 2020.

[11] U.A. Latif, "IceRayTracing." https://github.com/uzairlatif90/IceRayTracing, 8, 2020.

[12] C.W. James, H. Falcke, T. Huege and M. Ludwig, *General description of electromagnetic radiation processes based on instantaneous charge acceleration in "endpoints"*, *Phys. Rev. E* **84** (2011) 056602.

[13] D. Van den Broeck, S. Buitink, K. de Vries, T. Huege and U. Latif, *Radio propagation in non-uniform media*, in *9th International Workshop on Acoustic and Radio EeV Neutrino Detection Activities — PoS ARENA2022 (2022) 020*, vol. 424.

[14] K.D. de Vries, A.M. van den Berg, O. Scholten and K. Werner, *The lateral distribution function of coherent radio emission from extensive air showers: Determining the chemical composition of cosmic rays*, *Astroparticle Physics* **34** (2010) 267.

[15] C. Glaser et al., *NuRadioMC: Simulating the radio emission of neutrinos from interaction to detector*, *Eur. Phys. J. C* **80** (2020) 77 [1906.01670].